OPTOELECTRONICS AND ADVANCED MATERIALS – RAPID COMMUNICATIONS Vol. 7, No. 11-12, November - December 2013, p. 976-979

Synthesis and structural, optical and thermal properties of ceria and rare earth doped ceria nanocrystals

M. KARL CHINNU[a,b*], K. VIJAI ANAND[d], R. MOHAN KUMAR[c], T. ALAGESAN[c], R. JAYAVEL[a]
[a]*Centre for Nanoscience and Technology, Anna University, Chennai-25, India*
[b]*Department of Physics, S.A. Engineering College, Chennai-77, India*
[c]*Department of Physics, Presidency College, Chennai-5, India*
[d]*Department of Physics, Sathyabama University, Chennai-119, India*

Single crystalline ceria and rare earth doped ceria nanoparticles have been successfully synthesized by sonochemical method using water solvent from aqueous solution containing $Ce(NO_3)_3.6H_2O$, $Gd(NO_3)_3{\cdot}6H_2O$, $Sm(NO_3)_3{\cdot}6H_2O$, NaOH and hexamethylenetetramine (HMTA) as a surfactant. Prepared CeO_2, $Gd:CeO_2$ and $Sm:CeO_2$ nanoparticles were dried in air oven at 100 °C for 24 h. The synthesized samples have been subjected to various characterization studies such as X-ray powder diffraction (XRD) for structural confirmation of fluorite cubic. The morphology of the prepared materials was studied by field emission scanning electron microscopy (FE-SEM). Thermo-gravimetric analysis (TG/DTA) reveals that ceria and doped ceria are thermal stable upto 400 ºC. UV-vis absorption of $Gd:CeO_2$ shows red shift, due to the electron- phonon interaction. Fluorescence studies show the emission peaks for ceria at 425 nm and gadolinium and samarium doped ceria at 466 nm.

(Received May 23, 2013; accepted November 7, 2013)

Keywords: Nanoparticles, Fluorescence, Thermo-gravimetric and HMTA

1. Introduction

Rare-earth oxides with different nanostructures are of great importance because of their prospective applications such as high-performance luminescent devices [1], biological labeling, and catalysts based on their electronic, optical and optoelectronic properties [2,3]. Among the rare earth oxides nanostructured ceria and ceria based materials have been the major focus of research because of their commercial applications such as oxygen sensors, semiconductor devices and solid electrodes in the solid oxide fuel cells utilizing their oxygen storage capacity [4]. Ceria nanoparticles are also used in high-energy efficiency for fuel-cells [5], polishing materials [6], additives in ceramics, and phosphors [7]. In recent years, efforts have been made on the synthesis of ceria and ceria based nanoparticles [8,9]. CeO_2 also act as absorbents of fluoride ion or arsenic based compounds and as a filter for ultraviolet rays [10]. Gadolinium and samarium doped ceria have demonstrated a high-ionic conductivity at moderate temperatures (500–750 °C) and are potential candidates as electrolyte in solid oxide fuel cell (SOFC) devices [11]. In the present investigation, a simple template sol-gel based Sonochemical technique has been adopted to prepare CeO_2, $Gd:CeO_2$ and $Sm:CeO_2$ nanoparticles from aqueous solution with HMTA as a surfactant. The morphology of the CeO_2, $Gd:CeO_2$ and $Sm:CeO_2$ hierarchical nanostructure and particle size can be changed by adjusting the reactant concentration, solvent and surfactant.

2. Experiment

Reagent grade $Ce(NO_3)_2{\cdot}6H_2O$, $Gd(NO_3)_3{\cdot}6H_2O$, $Sm(NO_3)_3{\cdot}6H_2O$ and NaOH were procured from Aldrich with 99.6% purity and used without further purification. Pure and doped (Gd & Sm) CeO_2 nanoparticles were synthesized by sonochemical method. At the precipitation stage, the homogeneous solution of 4 mol.% of NH_4OH or NaOH was added drop-wise to a stirred solution of 0.2 mol.% $Ce(NO_3)_3{\cdot}6H_2O$ dissolved in water solvent followed by heating at 70 °C until the pH of the solution was stabilized at >11. The surfactant of hexamethylenetetramine (HMTA) was added with dissolved cerium (III) nitrate solution and continuous stirring for 1h. Similarly $Gd:CeO_2$ and $Sm:CeO_2$ were synthesized, when 0.02 mol. % of gadolinium (III) nitrate or/ and samarium (III) nitrate was added with 0.18 mol. % of cerium (III) nitrate solution. The synthesized samples were centrifuged, washed several times using distilled water and ethanol. The prepared samples were dried in air oven at100 °C for 24 h and annealed at 300 °C for 8 h.

The products were characterized by using Siemens 5005 Powder X-ray diffractometer (XRD) with Cu Kα radiation for structural confirmation.The field emission scanning electron microscopy (FE-SEM) study with a JEOL 6300F microscope at an acceleration voltage of 3–5 kV was carried out. UV-vis absorbance spectra were obtained using a (CARY 500) Scan UV–Vis-NIR spectrophotometer. Fluorescence emission spectra were recorded at room temperature using Perkin Elmer LS 5B fluorescence spectrophotometer over the range 250–600

nm. TG-DTA analyses were performed with SII TG/DTA 6300 EXSTAR apparatus at a heating rate of 20 °C/min under N_2 atmosphere.

3. Results and discussion

3.1 Structural analysis

Fig. 1 shows X-ray diffraction patterns recorded for cerium oxide, gadolinium and samarium doped cerium oxide nanoparticles using water solvent with HMTA as a surfactant. The broad peaks indicate the synthesized materials are in nanosize. XRD spectra of HMTA capped samples show reduced peak intensity and broadening, which indicate that HMTA was capped on the nanoparticles by controlling further growth. The crystallite size was estimated for all synthesized samples using Scherrer's Equation [12].

$$D = \frac{0.89\lambda}{\beta \cos\theta} \quad (1)$$

Where D, λ, θand βare the crystallite size, X-ray wavelength of 0.1541 nm, Bragg diffraction angle and full width at half maximum of the diffraction peak respectively.

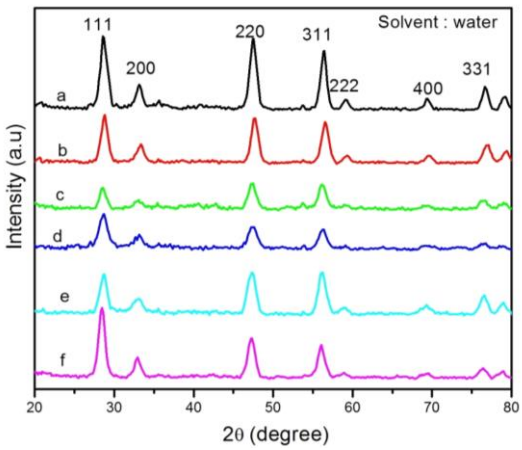

Fig. 1. XRD patterns of (a) pure CeO_2, (b) HMTA capped CeO_2, (c) Gd:CeO_2, (d) HMTA capped Gd:CeO_2, (e) Sm:CeO_2 and (f) HMTA capped Sm:CeO_2 nanoparticles.

The average crystallite size of ceria and rare earth doped ceria for water solvent is approximately 15-25 nm. On capping with HMTA, the crystallite size decreased systematically as shown in Table1. From the positions of the Bragg reflections, it is impossible to derive a unique set of lattice parameters for nanocrystals [13], because the 'apparent' lattice parameters, which depend on the diffraction vectors Q (Q = 2π /d, where d is the lattice inter spacing) can be used to distinguish the surface and bulk structures [14]. For nanocrystals, large Qs are more sensitive to the core and conversely, smaller Qs are less sensitive to the surface. With this result, several reflections, (111), (200), (220), (311), (222) (400) and (331) are selected to examine the surface and bulk effects. Positions of the Bragg peaks were determined from profiles fit to the experimental data.

Table 1. Average crystalline size and Q-factor for CeO_2 and rare earth doped CeO_2 nanoparticles.

Sample / Water solvent	2 theta (degree)	'd' spacing (nm)	Q - factor	FWHM	Crystallite size (nm)	Average crystallite size (nm)
Pure CeO_2	28.573	3.115	2.01	0.757	20.6	24.4
	47.5	1.91	3.29	0.873	23.26	
	56.38	1.68	3.74	0.87	28.4	
HMTA capped CeO_2	28.752	3.096	2.02	0.921	16.96	20.8
	47.78	1.905	3.3	1.012	20.16	
	56.554	1.63	3.86	0.982	25.28	
Pure Gd:CeO_2	28.56	3.13	2.01	0.913	17.1	21.56
	47.44	1.914	3.28	0.93	21.8	
	56.567	1.636	3.84	0.964	25.8	
HMTA capped Gd:CeO_2	28.646	3.112	2.02	0.969	16.12	21
	47.45	1.915	3.28	0.94	21.42	
	56.14	1.633	3.85	0.96	25.53	
Pure Sm:CeO_2	28.44	3.133	2.00	0.891	17.5	18.5
	47.325	1.916	3.27	1.257	16.1	
	56.23	1.637	3.83	1.08	22.12	
HMTA capped Sm:CeO_2	28.66	3.133	2.00	0.892	17.45	19.75
	47.26	1.92	3.27	0.965	20	
	56.077	1.638	3.84	1.12	21.8	

The results for CeO_2 and rare earth doped CeO_2 nanocubic structures are summarized in Table 1. Due to capping the crystalline structure is perfect with reduced grain size, and with rare earth doping the d-spacing may be changed because of the crystalline imperfection. In both the cases, it is clearly observed that the 'apparent'd-spacing are different for different Q values. In fact, the ratio of d-spacing (d/d_0 relative to ambient doping) for smaller Qs varies much less than those at higher Qs.

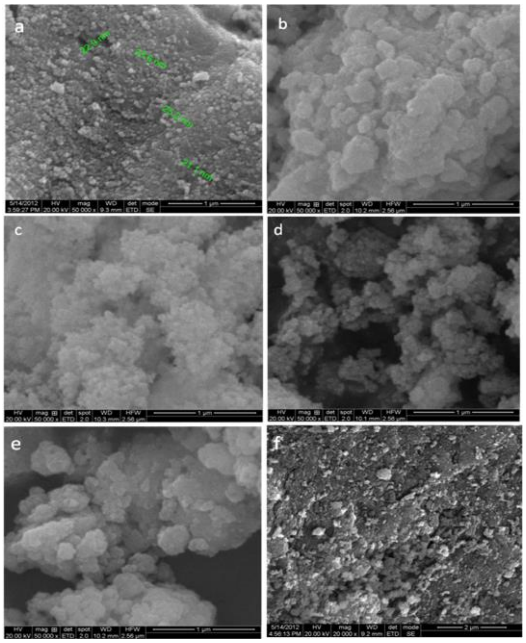

Fig. 2. FE-SEM images of (a) pure CeO_2, (b) HMTA capped CeO_2, (c) Gd:CeO_2, (d) HMTA capped Gd:CeO_2, (e) Sm:$CeO_2$and (f) HMTA capped Sm:CeO_2 nanoparticles.

Fig. 2 shows FE-SEM images of ceria and RE doped ceria with HMTA capped nanoparticles prepared using water solvent. The surface morphology of the ceria, gadolinium and samarium doped ceria reveals fine particles and/or local agglomerates. Fig. 2(a-f) shows the images of pure ceria, HMTA capped ceria, Gd and Sm doped ceria nanoparticles of about 20-30 nm in size prepared using water solvent. The capping agent relatively controls the uniform growth of nanoparticles with different concentration. HMTA capped ceria, Gd and Sm doped ceria nanoparticles possess reduced size. A relatively uniform surface appearance was evident for HMTA capped material with less concentrated sols. FE-SEM results were compared with XRD results and there was good agreement of particle size from both the studies. FE-SEM images also show morphologies of agglomerated particles and surface of the nanocrystal structures.

3.2 Optical properties

As an ultraviolet blocking material, CeO_2 nanocrystals have strong absorption properties in the ultraviolet range. Fig. 3 shows the UV-vis absorption spectra of pure and HMTA capped CeO_2 and rare earth doped CeO_2 nanoparticles, synthesized through sonochemical route using water as a solvent. For pure CeO_2, there is a strong absorption edge band at 394 nm (3.14 eV) (peak at 300nm), which is due to the charge-transfer transition from O^{2-}(2p) to Ce^{4+} (4f) orbital in the energy level. When CeO_2 nanoparticles were capped with HMTA, a strong absorption edge band at 430 nm (2.88 eV) was observed and it exhibited a red shift compared with that of pure CeO_2 nanocrystal. As for the red-shift, it could be the result of an interfacial polaron effect arising from electron–phonon coupling [15]. Similarly for Gd and Sm doped CeO_2 nanoparticles, the edge band absorptions were observed at 380 nm (3.26 eV) and 404 nm (3.07 eV) respectively. When HMTA capped Gd:CeO_2 and Sm:CeO_2 a slight change in edge band absorption occurs, which is blue shifted in comparison with the band gap of uncapped.

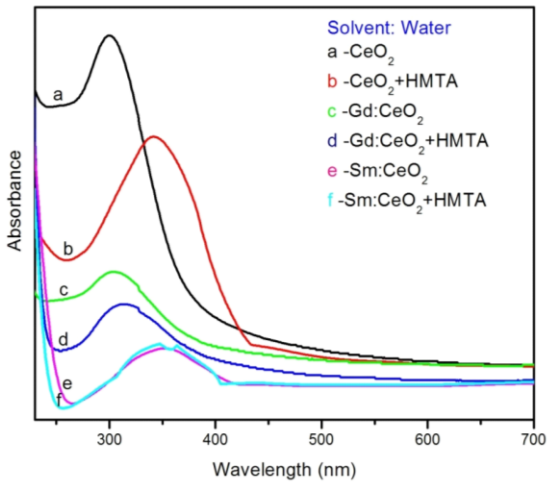

Fig. 3. UV-vis absorbance spectra of (a) pure CeO_2, (b) HMTA capped CeO_2, (c) Gd:CeO_2, (d) HMTA capped Gd:CeO_2, (e) Sm:CeO_2 and (f) HMTA capped Sm:CeO_2 nanoparticles.

The fluorescence study derives information on different energy states available between valence and conduction band and this is responsible for radioactive recombination. Fig. 4(A) shows the fluorescence spectra of pure CeO_2, Gd:$CeO_2$and Sm:CeO_2 nanoparticles and Fig.4(B) shows the HMTA capped CeO_2, Gd:CeO_2 and Sm:CeO_2 nanoparticles. The spectra were recorded at room temperature for pure and HMTA capped CeO_2 nanoparticles at an excitation wavelength of 350 nm. The fluorescence emission peaks for pure and HMTA capped CeO_2 lies at 406 nm and 430 nm. Similarly the fluorescence spectra of uncapped Gd:CeO_2 and Sm:CeO_2 the strong emission peaks at 435 nm and 466 nm respectively. For HMTA capped Gd:CeO_2 and Sm:CeO_2 nanomaterials the emission peaks observed at 435 nm and 466 nm. In addition, an emission peak was observed at 410 nm, due to the capping effect.

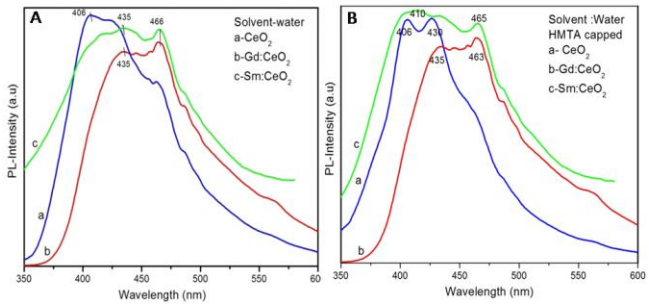

Fig. 4. (A,B) Fluorescence spectra of pure and HMTA capped (a) CeO_2, (b) Gd:CeO_2 and (c) Sm:CeO_2 nanoparticles.

3.3 TG /DTA analysis

To analyze the thermal properties of the precursor, the simultaneous TG/DTA analysis was performed and the results are given in Fig. 5. In order to completely remove the by-product of the precipitation reaction and excess water, moisture and organic compounds, the precursor was washed using 2D water and alcohol for three times and then dried at 100 °C. Fig. 5(a) shows the thermal behaviour of CeO_2 prepared with water solvent. A sudden weight loss occurs in the low temperature range 30-150 °C due to the removal of water and organic compounds and a gradual weight loss was observed between 150°C and 800 °C. There are two exothermic peaks in the corresponding DTA curves at 190 °C and 300 °C, and a gradual endothermic peak observed at 650°C. The average weight loss was 3%. For HMTA capped Sm:CeO_2 prepared using water solvent (Fig. 5(b)), the TGA curve indicate gradual weight loss upto 800 °C. A gradual endothermic peak at 280 °C and gradual exothermic at 800°C due to the decomposition and the total weight loss was observed 6 %.

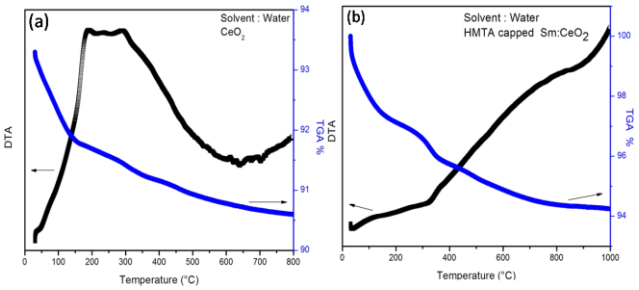

Fig. 5(a,b). Simultaneous TG/DTA curves of as prepared pure CeO_2 and HMTA capped Sm:CeO_2 using water solvent. The data measured in air at a heating rate of 20 °C/min.

4. Conclusion

CeO_2, Gd:CeO_2 and Sm:CeO_2 nanoparticles were prepared by sonochemical technique. HMTA capped CeO_2, Gd:CeO_2 and Sm:CeO_2 nanoparticles were small change in size than the uncapped nanoparticles and exhibit as a fluorite cubic structure as evident from the XRD and FE-SEM studies. The blue-shift in the UV-vis absorption for doped and capped CeO_2 nanomaterials may be ascribed to the quantum size effect. CeO_2 nanoparticles capped with HMTA, show strong absorption edge bands at 430 nm (2.88 eV) and 446 nm (2.78 eV). The fluorescence efficiency of the HMTA capped nanocrystals was reduced dramatically by localized surface trap states. The blue/green ratio decreases as the doping with samarium, whereas ionic conductivity increases with samarium doping. The thermal stability of CeO_2, Gd:CeO_2 and Sm:CeO_2 studied, Sm:CeO_2 has high thermal stability.

References

[1] R. M. Ormerod, Chem. Soc. Rev., **32**, 17 (2003).
[2] L. H. Slooff, A.Van-Blaaderen, A. Polman, G. A. Hebbink, S. I. Klink, F. C. Van Veggel, J. M., Reinhoudt, D. N. Hofstraat, J. W., J. Appl. Phys., **91**, 3955 (2002).
[3] P. Patsalas, S. Logothetidis, C. Metaxa, Appl. Phys. Lett. **81**, 466 (2002).
[4] D. J. L. Brett, A. Atkinson, N. P. Brandon, S. Skinner, J. Chem. Soc. Rev., **37**, 1568 (2008).
[5] Z. Shao, J. Mederos, W. C. Chueh, S. M. Haile, J. Power Sourc., **162**, 589 (2006).
[6] L. Seung-Ho, L. Zhenyu, S. V. Babu, E. Matijevic, J. Mater. Resear., **17**, 2744 (2002).
[7] S. Tsugio, Ruixing, Li, S. Chigusa, Y. Shu, Phosphor. Resear. Bulletin, **21**, 44 (2007).
[8] J. Zhang, X. Ju, Z. Y. Wu, T. Liu, T. D .Hu, Y. N. Xie, Z. L.Zhang, Chem. Mater., **13**, 4192 (2001).
[9] F. Zhang, S. W. Chan, J. E. Spanier, E. Apak, J. Qiang, D. Richard, Robinson, I. P. Herman, Appl. Phys. Lett., **80**, 28 (2002).
[10] N. Zhang, L. Siqi, F. Xianzhi, X. Yi-Jun, J. Phys. Chem. C, **115** (46), 22901(2011).
[11] J. Prado-Gonjal, R. Schmidt, J. Espíndola-Canutoa, P. Ramos-Alvarez, E. Morán, J. Power Sourc., **209**, 163 (2012).
[12] L. Sapanhel, M. A. Anderson, J. Amer. Chem. Soc., **112**, 2278 (1990).
[13] J. Zhang, Y. Zhao, B. Palosz, Appl. Phys. Lett., **90**, 43112 (2007).
[14] M. Y. Ge, Y. Z. Fang, H. Wang, W. Chen, Y. He, E. Z. Li, N. H. Su, P. Feng, J. S. Tse, T. Kikegawa, S. Nakano, Z. L. Zhang, U.Kaiser, F. M.Wu, H-K. Mao, Jiang, New Phys., **10**, 1 (2008).
[15] S. Sathyamurthy, K. J. Keith Leonard, R. T. Dabestani, M. P. Paranthaman, Nanotechnology, **16**, 1960 (2005).

*Corresponding author: chinnu0202@gmail.com